J Solid State Electrochem (2018) 22:1539–1548
DOI 10.1007/s10008-017-3774-1

ORIGINAL PAPER

The iron oxyhydroxide role in the mediation of charge transfer for water splitting using bismuth vanadate photoanodes

Moisés A. de Araújo[1] · Dyovani Coelho[1] · Lucia H. Mascaro[1] · Ernesto C. Pereira[1]

Received: 10 July 2017 / Revised: 12 September 2017 / Accepted: 17 September 2017 / Published online: 27 September 2017

Abstract The water photo-oxidation to oxygen on iron oxyhydroxide (FeOOH) deposited on a surface of semiconductor materials play a crucial role in the enhancement of different devices. In order to investigate how FeOOH works to produce O_2 from water splitting, we have investigated the role of a deposited layer of FeOOH on the bismuth vanadate ($BiVO_4$) films. The simple-modified method based on polyethylene glycol was applied to produce $BiVO_4$ nanostructures and a FeOOH photoelectrodeposition methodology was used to cover the $BiVO_4$ film surface. The photoelectrochemistry study for FeOOH modified $BiVO_4$ revealed a 3.4 times increase in the photocurrent at 1.23 V vs. RHE. A possible explanation to the FeOOH mechanism is that it is actually a green rust containing a mixture of Fe (II) and Fe (III) that acts as center of charge transfer mediation and not as a catalyst itself. This hypothesis has been supported by a change absence in the onset potential, no photocurrent saturation, and no change in the charge carrier density. Moreover, the FeOOH also passivated the surface states of $BiVO_4$ as the open circuit potential shifted 70 mV vs. RHE to more positive potentials.

Keywords Bismuth vanadate · Iron oxyhydroxide · Water splitting · Hydrogen · Energy · Photoelectrochemical cell

✉ Ernesto C. Pereira
ernesto@ufscar.br

[1] Department of Chemistry, Federal University of São Carlos, Rodovia Washington Luiz, km 235, CEP, São Carlos, SP 13565-905, Brazil

Introduction

Applying semiconductor materials in photocatalysis have been one of the most promising ways to produce hydrogen gas (H_2) via water splitting. Since the initial studies used TiO_2 [1] for such purposes, different materials have been proposed. In this sense, bismuth vanadate ($BiVO_4$), an n-type semiconductor, is a highly promising candidate to produce oxygen gas (O_2). The holes produced can be used to oxidize water into O_2 [2]. Considering $BiVO_4$, it presents two stable phases, the tetragonal and the monoclinic scheelite phase, and the latter is the most photoactive crystalline phase, which presents a narrow direct band gap ≈ 2.4 eV [3, 4] that covers a great portion of the visible electromagnetic spectrum. Furthermore, $BiVO_4$ also presents low toxicity and it is composed by abundant elements [5].

Given the great importance of the $BiVO_4$ crystalline structure, many methods have been reported to synthesize monoclinic $BiVO_4$, such as electrodeposition [6], organic-metal decomposition [7–9], hydrothermal synthesis [10, 11], spray pyrolysis [12], solid state reaction [13], co-precipitation [14], and chemical vapor deposition [15]. In general, the process of $BiVO_4$ synthesis requires a great deal of energy and/or involves several steps. In our group, Mascaro et al. [16] developed a simple and one-way step to produce $BiVO_4$ films using polyethylene (PEG) 300 to dissolve the precursor reagents. Other authors have also applied PEG to obtain $BiVO_4$ [17–19]. The use of PEG as a solvent plays an important role on the porosity of the material [19], as well as the particles size [17]. The consequence of morphological modifications such as porosity and particle size would dramatically affect the photoelectrocatalysis performance of the semiconductor material.

Although $BiVO_4$ is a material with great potential to produce O_2, the electron-hole recombination pairs, low electron

conductivity, and reduced hole transfer kinetics to the water oxidation [6] are still hurdles to fully fulfill the photocurrent or photon to oxygen conversion efficiency of the pure material. Modifying the surface of $BiVO_4$ with an oxygen evolution catalyst (OEC) [6] has demonstrated to be one of the most convenient ways to overcome this problem. The OEC combined with $BiVO_4$ are mainly cobalt-phosphate (Co-Pi) [20, 21] and metal-based oxides such as RhO_2 [22], and PdO_x [23]. Other classes of OEC are the metal-based oxyhydroxide (MOOH) as NiOOH [24] and FeOOH [24–28].

Photodeposition [24, 25] is one of the methods reported to obtain an FeOOH layer on $BiVO_4$; such methodology was applied in this report with modifications. Photodeposition is based on oxidizing Fe (II) to Fe (III) by the photogenerated holes. Then, the Fe (III) ions precipitate as FeOOH on the $BiVO_4$ film. This approach brings as an advantage to place OEC mostly where holes are likely available to the water photo-oxidation on a semiconductor surface. According to the literature, the presence of FeOOH on $BiVO_4$ results in a dramatic increase of the photocurrent, which is ascribed to the collection of photogenerated holes from $BiVO_4$ layer by FeOOH. Besides, the onset potential is shifted in a negative direction indicating that the kinetics of oxygen evolution is enhanced and the recombination is suppressed [25]. FeOOH has also prepared over different semiconductor surfaces, such as hematite [29]. Kim et al. [29] attributed the enhancement of water oxidation to O_2 due to the passivation of the surface states of the hematite, which consequently increased the charge separation efficiency.

Despite of the significant improvement of photocatalysis properties, FeOOH has been less explored than Co or Ni based OEC [6]. Moreover, very little is known regarding FeOOH mechanism action on the enhancement of O_2 evolution kinetics on the surface of $BiVO_4$. That said, the aim of this report is to contribute in the investigation of the role of FeOOH on $BiVO_4$ applied to water splitting, and furthermore, to investigate the optoelectronic and structural properties of $BiVO_4$ and $BiVO_4$/FeOOH nanostructured films.

Experimental

Synthesis of $BiVO_4$ films

$BiVO_4$ thin films were prepared by the modification of the methodology previously reported in our group [16]. The precursors NH_4VO_3 (0.1182 g) and $Bi(NO_3)_3.5H_2O$ (0.4950 g) were dissolved separately in 2.5 mL of a mixture 1:1 of polyethylene glycol 300 and ethylene glycol, and were stirred for 30 min. The precursor solutions were then combined and stirred for another 30 min. To obtain the films by spin coating, 50 μL of the suspension was dropped on a cleaned and hydrophilized FTO and subsequently spun at 1000 rpm for 30 s. This procedure was repeated seven times; at the end the films were annealed in air at 500 °C for 1 h.

Synthesis of $BiVO_4$/FeOOH films

The surface modification of the photoanode with the OEC was obtained by the photoelectrodeposition of FeOOH on $BiVO_4$ films in a $FeSO_4$ solution, which was a modification of the methodology reported elsewhere [24]. Initially the following deposition parameters were investigated in order to obtain the highest photocurrent: (i) applied potential (0.4, 0.6, 0.8, and 1.0 V vs. Ag/AgCl/$KCl_{Sat.}$), (ii) deposition time (5, 30, and 60 min), (iii) $FeSO_4$ concentration (0.001 mol L^{-1} pH 5.4 and 0.1 mol L^{-1} pH 4.0), and (iv) applying or not 1.2 V vs. Ag/AgCl/$KCl_{Sat.}$ after photoelectrodeposition. The optimized conditions consisted in photoelectrodeposition under back-side illumination of the FTO/$BiVO_4$ photoanode (on glass face of FTO) into $FeSO_4$ 0.1 mol L^{-1} solution for 30 min applying 0.4 V vs. Ag/AgCl/$KCl_{Sat.}$ in order to facilitate the deposition of FeOOH. In this conditions was obtained a deposition charge of 154 ± 26 mC cm^{-2}. The photoelectrodeposition was carried out in a three-electrode cell containing $BiVO_4$ as a working electrode, a Pt counter electrode, and an Ag/AgCl (KCl saturated) reference electrode. The light source was a 150 W xenon lamp with AM 1.0G filter and radiance of 100 mW cm^{-2}.

Characterization of $BiVO_4$ and $BiVO_4$/FeOOH films

The X-ray diffraction (XRD) pattern of the $BiVO_4$ and $BiVO_4$/FeOOH films were carried out on a Shimadzu XRD-6000 X-ray diffractometer with Cu Kα radiation (λ = 1.54 Å), in the 2θ range of 15° to 60° at a scanning rate of 1°s^{-1}, and an accelerating voltage of 30 kV. The morphologies of the films were investigated by high-resolution field emission scanning electron microscopy (FE-SEM, Zeiss Supra 35 at 5 kV), and the chemical analysis of the films were performed on a FE-SEM Inspect F50 with EDAX. In order to estimate the optical band gap of the semiconductors, UV-vis spectra were obtained using a Varian Cary 5G UV-vis-NIR spectrophotometer in the diffuse reflectance mode.

Photoelectrochemical and electrochemical measurements

The photocurrent measurements were conducted in the same electrochemical cell and with the same light source as described previously for the FeOOH photoelectrodeposition. The experiments were performed in Na_2SO_4 0.5 mol L^{-1} solution at pH 5.60. The linear voltammetric profiles were recorded at 20 mV s^{-1} sweeping the potential to more positive values. The area illuminated of the films was ≈ 1 cm^2. All the photoelectrochemical measurements were carried out with Ag/AgCl (KCl saturated) reference electrode, and the results

were presented against the reversible hydrogen electrode (RHE) as that would allow an easy comparison of the data with the others in the literature. The conversion of the potential scale was calculated applying the following equation.

$$E_{(vs.\mathrm{RHE})} = E_{(vs.\mathrm{Ag}/AgCl/\mathrm{KCl\ sat.})} + E_{(\mathrm{Ag}/AgCl/\mathrm{KCl\ sat.})\mathrm{ref}} + (0.059 \times \mathrm{pH})$$

$$E_{(\mathrm{Ag}/AgCl/\mathrm{KCl\ sat.})\mathrm{ref}} = 0.197\ \mathrm{V}\ vs.\mathrm{RHE\ at\ 25}^{o}\mathrm{C}$$

Tests in buffered solution at the same pH (5.6) demonstrated that the shift of polarization curves of the $BiVO_4$/FeOOH did not exceed 80 mV to the onset potential of photocurrent, while the absolute values of photocurrent densities at 1.23 V vs. RHE were similar, where into buffered solution the photocurrent was 4.8% higher than into non-buffered electrolyte. Some papers about WO_3 and $BiVO_4$ photoanodes also reported such changes when the parameters of solutions as concentration, pH, or salt used as electrolyte are changed [30–33]. In agreement with the literature, this occurs due to the differences between anions adsorption on photoanode surface, which could change the kinetics of charge transfer at the interface photoanode/electrolyte.

To obtain the Mott-Schottky plots, the capacitance of $BiVO_4$ and $BiVO_4$/FeOOH films were measured. The sinusoidal modulation applied was 10 mV with a frequency of 1 kHz.

In order to evaluate the charge transfer resistance at the interface semiconductor/electrolyte, an electrochemical impedance spectroscopy was performed in the frequency range of 10 kHz to 0.2 Hz with 10 mV of amplitude. This experiment was conducted under illumination and at the open circuit potential (E_{ocp}), which was 0.70 and 0.77 V vs. RHE for $BiVO_4$ and $BiVO_4$/FeOOH, respectively. All the electrochemical experiments were performed using the Potentiostatic Autolab PGSTAT302N.

Results and discussion

The phase with higher photoactivity of $BiVO_4$ is the monoclinic scheelite; however, the semiconductor can present a tetragonal phase too. Therefore, the photoanodes were characterized by an X-ray diffraction to find out its crystalline structure; the diffraction patterns are shown in Fig. 1. The diffraction peaks are indexed with the monoclinic phase of $BiVO_4$ (JCPDS No 75–1867) with cell parameters a = 5.195 Å, b = 5.093 Å, and c = 11.704 Å and space group I2/b. There is no preferential orientation growth of $BiVO_4$ on FTO, as the relative intensities of the peaks are similar to those of the standard diffractogram. The average crystallite size obtained from the Scherrer equation applied to the diffraction peak at 28.96° (two theta) is 35 nm. Besides that, the splitting of peaks at 18.9°, 35°, and 47° observed is characteristic to the monoclinic structure, which confirms that this phase is obtained in the pure form after heat treatment without a mixture of the tetragonal scheelite structure [16, 34]; the characteristic peak of tetragonal phase (JCPDS No 14–133) at 24° was not observed. The peaks identified with asterisks are related to the FTO substrate (PDF No 88-287) [35]. The analysis of the diffraction pattern shows a small shifting of the peaks, about 0.2° to the pure $BiVO_4$ film and 0.1° to the substrate (using the software Crystallographica Search-Match, version 2, 1, 1, 1). Probably this fact occurs because of strain effect [36] in the thin film, with 750 ± 90 nm of thickness calculated from the cross section image of SEM showed in Fig. 2.

Although the X-ray patterns did not show differences for the films modified with the FeOOH photoelectrodeposited, the microscopic images indicated a change of morphology after the deposition of the OEC. The images of SEM in Fig. 2 for the semiconductor film before photoelectrodeposition of FeOOH exhibit wormlike-shaped particles with an average size of 140 ± 46 nm. After the photoelectrodeposition of FeOOH on $BiVO_4$ the image displays the coalescence of small particles, like spheres, on the wormlike-shaped particles. The same patterns of images were obtained by Kim and Choi [37] when evaluating the photoelectrochemical behavior of $BiVO_4$ films modified with $ZnFe_2O_4$. One of the steps during the deposition of $ZnFe_2O_4$ was the photoelectrodeposition of FeOOH. It is believed that these particles are amorphous FeOOH, and they are deposited over the surface of $BiVO_4$ exposed to the electrolyte solution containing Fe (II). To compare, after FeOOH deposition on FTO, the same pattern is observed, showing small particles on FTO. The thickness of the $BiVO_4$ film is 750 ± 90 nm, approximately, and there is not significant change after photoelectrodeposition of FeOOH. The mechanism of the photoelectrodeposition of FeOOH on $BiVO_4$ is based on the use of photogenerated holes to oxidize Fe (II) ions to Fe (III) ions producing the FeOOH insoluble, which remains adsorbed on the $BiVO_4$ layer [27]. The pH of the medium is controlled to keep Fe (II) ions dissolved, though it is not enough to dissolve the amorphous particle of FeOOH. However, it is believed that the photoelectrodeposition yields a kind of green rust sulfate containing Fe (II) and Fe (III), which is discussed in more detail to propose the charge transfer mediation during the photoelectrochemical oxidation of water.

In order to confirm the presence of the iron compounds in the particles, EDS analysis was performed and the EDS spectra as the mapping are shown in Fig. 3. It is noted the presence of the iron in the EDS spectra (Fig. 3a), however in low quantity, which as expected because of the SEM images show a thin layer of particles coating on $BiVO_4$ surface. The elementary mapping in Fig. 3b exhibited a homogeneous distribution of iron compounds throughout the surface of $BiVO_4$ film.

The optical band gap was estimated using the diffuse reflectance spectroscopy (DRS) and the Kubelka-Munk function to determine the absorption coefficient of the

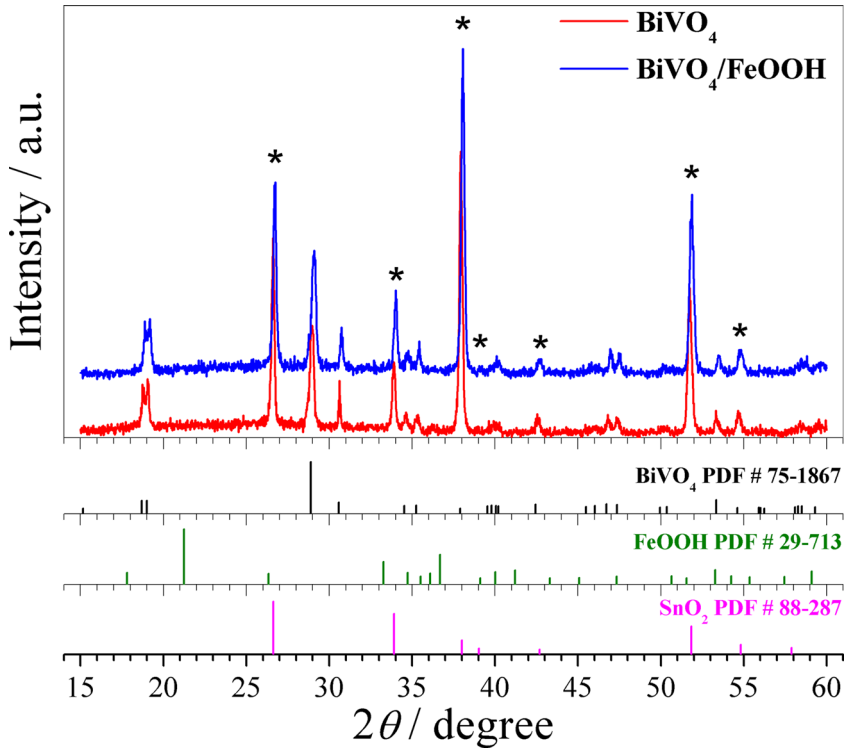

Fig. 1 Diffraction patterns of $BiVO_4$ and $BiVO_4$/FeOOH films

semiconductor film [38]. It was concerning that both films, $BiVO_4$ and $BiVO_4$/FeOOH, were semiconductors of direct interband transitions. Figure 4 shows the reflectance diffuse spectrum and the Tauc plot for FTO, FTO/$BiVO_4$, and FTO/$BiVO_4$/FeOOH films. The band gap of semiconductor films are in agreement with those reported in literature [3, 4] and was not observed to have any significant difference after the photoelectrodeposition of FeOOH on the $BiVO_4$ film [16]. The films present optic band gaps of 3.74, 2.59, and 2.57 eV to FTO, $BiVO_4$, and $BiVO_4$/FeOOH, respectively (insert of

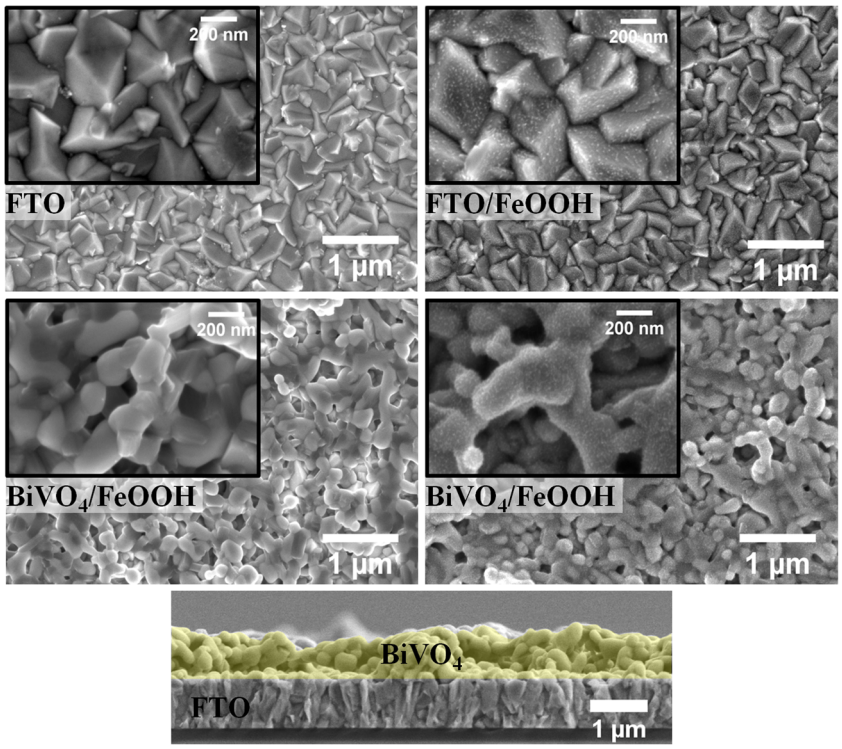

Fig. 2 SEM images of FTO and $BiVO_4$ films before and after FeOOH photoelectrodeposition

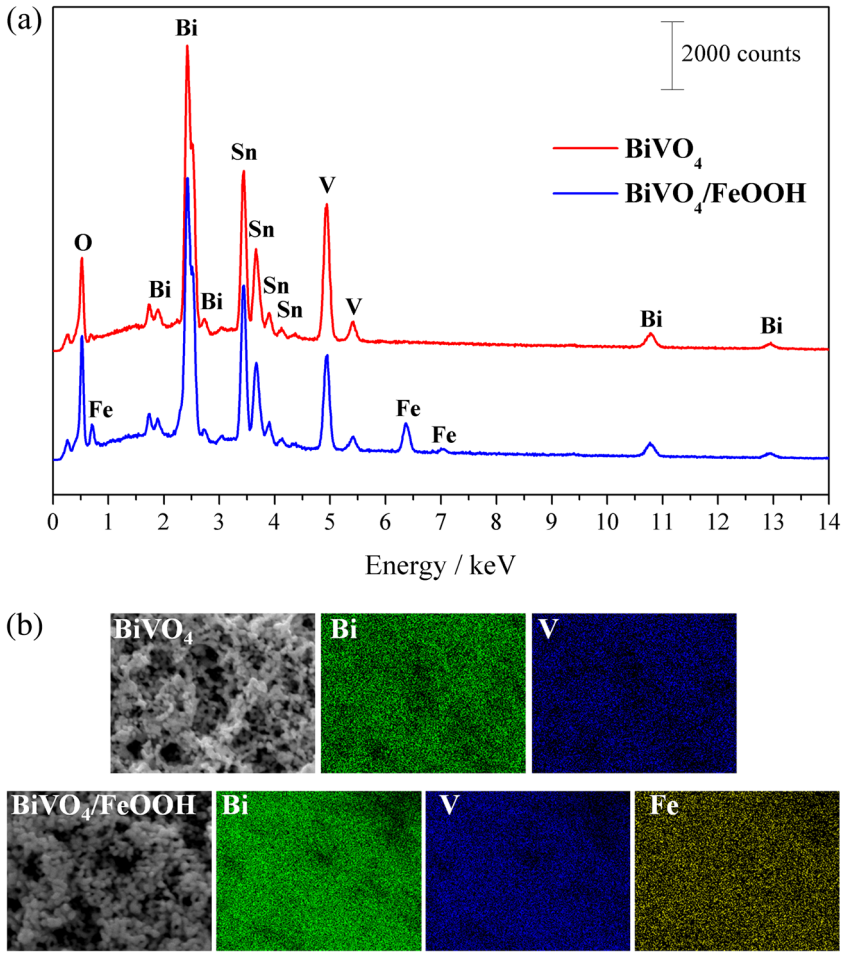

Fig. 3 **a** EDS spectra and **b** EDS mapping of the $BiVO_4$ and $BiVO_4$/FeOOH films

Fig. 4). Despite the fact that FeOOH does not contribute to the decrease of the band gap, the photocurrent is greatly influenced by that step.

Figure 5 shows the linear voltammograms of $BiVO_4$ and $BiVO_4$/FeOOH under dark and illuminated conditions; all the

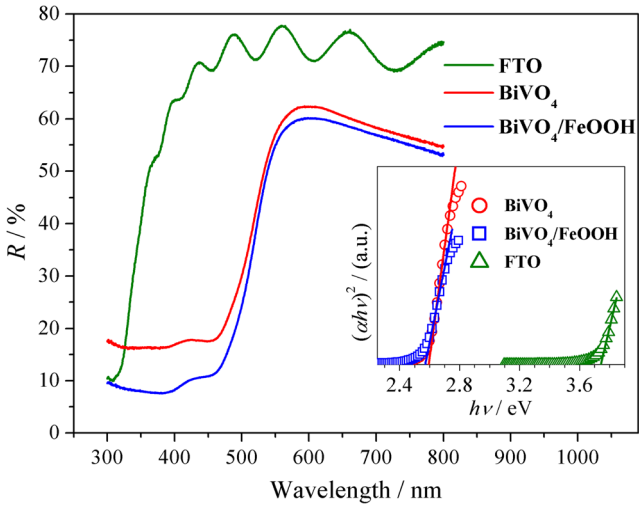

Fig. 4 Diffuse reflectance spectra and Tauc plots (insert) of $BiVO_4$/FeOOH, $BiVO_4$, and FTO

films were back-side illuminated through FTO, as it provides a much higher density of photocurrent than front illumination. The oxidation wave between 0.65 and 1.20 V is attributed to vanadium oxidation [16]. Furthermore, in the same range of potential it is observed a decrease in current density to $BiVO_4$/FeOOH under dark conditions, which is associated with the coverage of the $BiVO_4$ surface with particles of FeOOH. This leads to the less exposure of the vanadium oxide. Therefore, the voltammetric profile is in agreement with the microscopic images of $BiVO_4$/FeOOH shown after the photoelectrodeposition of FeOOH. Under illumination the photocurrent density of the pure $BiVO_4$ film is about 148 ± 27 μA cm^{-2} at 1.23 V, while the $BiVO_4$/FeOOH film presents a value of 507 ± 56 μA cm^{-2}, an increase of approximately 3.4 times in the photocurrent density. The gain in the density of photocurrent cannot be ascribed to differences in the band gap or to the thickness of films, as they are very similar for both $BiVO_4$ and $BiVO_4$/FeOOH. Likewise, the increase cannot be attributed to light absorption by FeOOH as pure films of this material on FTO did not show any photoactivity. Therefore, the main reason for the density of photocurrent increases is due to the role of FeOOH in the water-splitting mechanism. Although in Fig. 5a, it may appear

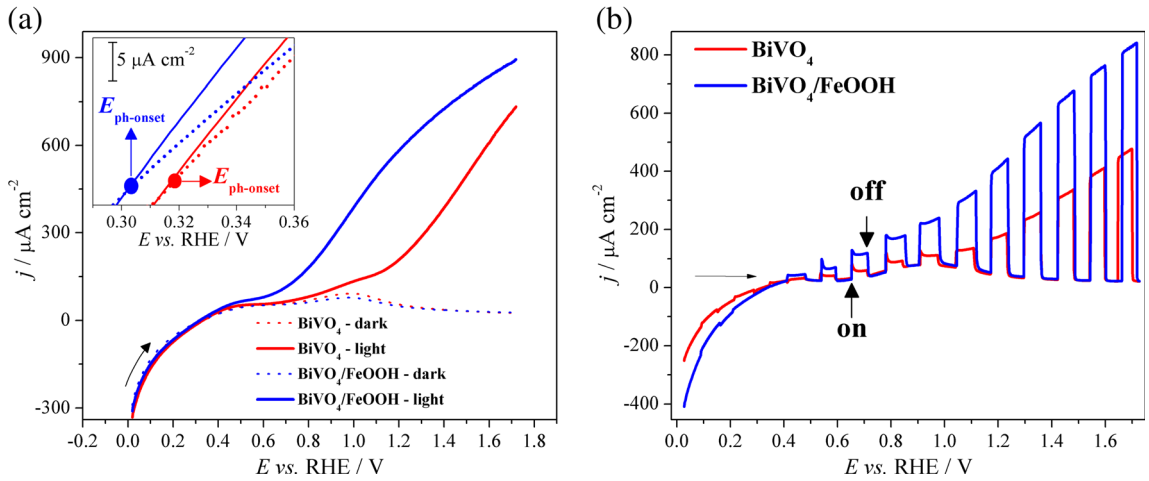

Fig. 5 **a** Linear voltammograms under dark and illumination. **b** Linear voltammograms under intermittent illumination. Measurements performed at 20 mV s^{-1} in Na_2SO_4 0.5 mol L^{-1} pH 5.6

that the $BiVO_4$/FeOOH exhibits a negative shift in the onset potential of photocurrent, there is no significant shift (insert of Fig. 5a), ≈ 10 mV. This is more evident in Fig. 5b, with linear voltammograms under intermittent illumination, where it is possible to observe that the onset photocurrent is the same for both photoanodes, $BiVO_4$ and $BiVO_4$/FeOOH, on the conditions of the measurement. The presence of FeOOH top layer only increases the photocurrent.

In the literature, there are few papers that discuss the mechanism of water oxidation evolving the FeOOH, and all of them impute this phenomenon to heterogeneous catalysis [24, 27, 39]. An explanation is proved by Seabold, Zhu, and Neale [39], who proposed that the FeOOH suppressed the interfacial states of the $BiVO_4$ layer. In other reports, Kim and Choi [24] suggest that the interface between the absorber layer and the OEC act as a center of recombination, and this is the cause of the photocurrent density not reaching a saturation point when compared to the photoresponse into a solution containing a scavenger such as sulfite. They attribute the increase of photocurrent density when $BiVO_4$ film is modified with the FeOOH layer to the higher charge transfer kinetic to water oxidation and changes in the flat band for more negative potentials with FeOOH deposition. The same explanation is supported by McDonald and Choi [27]. In a recent study made by Kim et al. [29], the authors obtained an over layer of FeOOH on the Fe_2O_3 photoanode and pointed out that the FeOOH works as a passive layer and increases the surface charge separation.

Chemelewski et al. [40] demonstrated the properties of FeOOH in its allotropic form, goethite, after its electrodeposition on FTO. The FeOOH acts as catalyst and presents overpotential for water oxidation much less than it does for FTO substrates. Additionally, the authors used the FeOOH as a protective layer onto light absorber material. In this case, they used a triple junction of amorphous silicon solar cell as light absorber material and FeOOH as catalyst and protective layer. This is in agreement with the reports by Kim et al. [29], who related that the FeOOH acted as a passive layer on the absorber. Besides that, the green rust could also act as a blocking layer, however as it was observed in the scanning microscopic electronic images, the $BiVO_4$ surface was not totally covered with green rust. Then, this is not the mainly effect for the increase of photocurrent. It is more plausible that the green rust works as a charge transfer mediator decreasing the hole accumulation at semiconductor/electrolyte interface. As we showed here, the FeOOH does not work as light absorber, but it increases the charge transfer at film's surface, which contributes to its stability and higher photocurrent (Fig. 6). The transient current displayed in Fig. 6 shows exactly this behavior; the photoanode containing FeOOH presents the highest density of photocurrent under illumination and a photocurrent density decays similar to $BiVO_4$. After 1.5 h of incident irradiation, the photocurrent density observed for $BiVO_4$/FeOOH is about 88 μA cm^{-2}, 2.5 times higher than pure $BiVO_4$. Once that occurs, the photocurrent density keeps stable for 1 h after the period of stabilization, and the FeOOH photoelectrodeposited particles could stay on surface of $BiVO_4$ film, otherwise the current could drop until the values observed to $BiVO_4$ film. The transient decay of the photocurrent density can be assigned to the decrease of local pH in the interface FeOOH/electrolyte that dissolves the FeOOH and causes the decreasing in the photocurrent density. The same behavior was observed by Seabold et al. [39], when they studied the $BiVO_4$ doped with Mo.

Here, we suggest that the centers containing iron act like mediators to electron transference on the surface decreasing the charge transfer resistance. In this case, the particles of FeOOH could not be stoichiometric, and they could have a mix of Fe (III) and Fe (II) yielding a kind of green rust, as the product of corrosion on metallic surfaces [41]. In agreement with Refait et al. [42] and Génin et al. [41], the green rust sulfate presents an oxidation number for Fe of + 2.33. Thus,

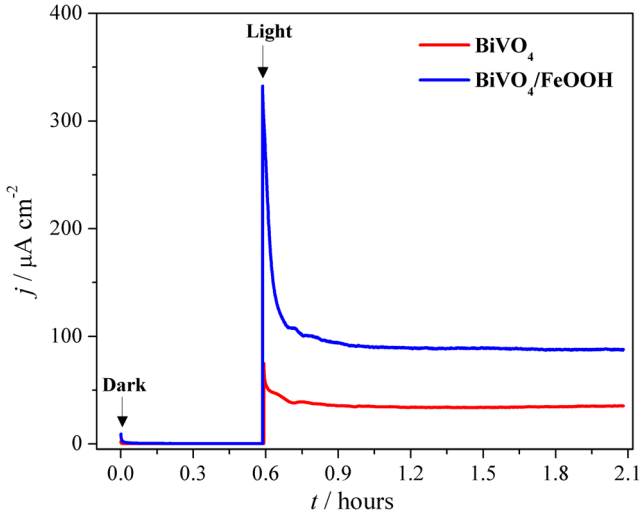

Fig. 6 Transient current density at 1.23 V under dark and sun light simulator of $BiVO_4$ and $BiVO_4$/FeOOH films. Measurements performed in Na_2SO_4 0.5 mol L^{-1} pH 5.6

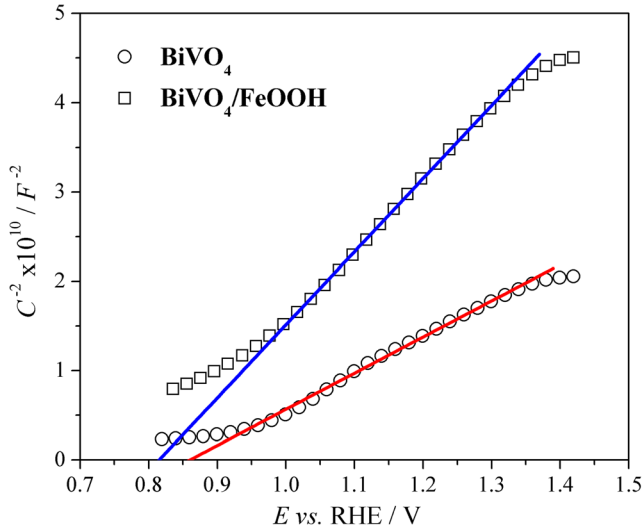

Fig. 7 Mott-Schottky plots of $BiVO_4$ and $BiVO_4$/FeOOH films. Measurements performed in Na_2SO_4 0.5 mol L^{-1} pH 5.6

the centers containing the mix of Fe (II)-Fe (III) can be oxidized by holes photogenerated in the space charge of $BiVO_4$ that reached the surface of the film and the water could be oxidized to O_2 by centers containing iron regenerating the green rusts. Consequently, the FeOOH layer mainly acts in the mechanism of the charge transfer at semiconductor/electrolyte interface. To investigate this phenomenon was determined the flat band potential (E_{fb}) and the charge carrier density (N_D) of the films using the Mott-Schottky plot presented in Fig. 7, which can be obtained from an analysis of the Mott-Schottky plot's linear region with the following equation:

$$\frac{1}{C_{SC}{}^2} = \left(\frac{2}{\varepsilon\,\varepsilon_0\,q\,N_D\,A^2}\right) \times \left(E - E_{fb} - \frac{k_B\,T}{q}\right)$$

where q is the elementary charge (1.602×10^{-19} C), ε is the semiconductor dielectric constant (32 for $BiVO_4$ and $BiVO_4$/FeOOH [43]), ε_o is the vacuum permittivity constant (8.85×10^{-14} F cm^{-1}), A is the electrode area (1.0 cm^2), k_B is the Boltzmann constant (1.38×10^{-23} J K^{-1}), T is the absolute temperature (298.2 K), and E is the applied potential [44]. Therefore, a $C_{SC}{}^{-2}$ vs. E plot can be used to determine the type semiconductor, the E_{fb} and the N_D. The type semiconductor is estimated from the slope (positive to n-type and negative to p-type semiconductor) and the E_{fb} from the intercept on the potential axis when the C_{SC} is zero. The value of N_D can also be determined from the slope, given the values of ε and A. The values obtained are shown in Table 1.

Table 1 shows a shift of 40 mV of the E_{fb} to negative potential when $BiVO_4$ is covered with FeOOH. As the band gap determined by DRS is almost the same for both films, $BiVO_4$ and $BiVO_4$/FeOOH, the shift of E_{fb} means that the potential of the valence band for the last one is more negative than for the pure semiconductor film. The N_D calculated to the $BiVO_4$ is higher than to the $BiVO_4$/FeOOH; therefore, the increase of photocurrent after the photoelectrodeposition of FeOOH does not follow the change at charge carrier density. This supports the hypothesis that the FeOOH acts as a charge transfer mediator and not as a catalyst itself or blocking layer, because a shift of the photocurrent onset potential was not observed in the voltammetric measurements, which is associated with a decrease in the activation energy of the reaction of water oxidation.

Actually, the Mott-Schottky model is not completely suitable for the film studied here, as the FeOOH top layer is not recovered throughout the $BiVO_4$ surface as shown in the SEM images. However, it is worth noting that the parameters determined to $BiVO_4$ pure film are reliable and comparable with the reported results in the literature even though the E_{fb} and N_D related in the literature can present a substantial dispersion depending on electrolyte, pH, and film deposition methods [22, 45, 46]. Thus, electrochemical impedance spectroscopy was performed at open circuit potential (E_{ocp}) to evaluate the charge transfer resistance at photoanode surface during water oxidation.

According to the charge transfer resistances measurements under dark and illumination conditions at E_{ocp}, the increase in the photocurrent shown after photoelectrodeposition of FeOOH on $BiVO_4$ is due to its mediation in charge transfer of holes from $BiVO_4$ to the electrolyte. The coverage of $BiVO_4$ surface with FeOOH expressively decreases the charge transfer resistance under illumination, as shown in the Fig. 8. In contrast to $BiVO_4$/FeOOH, the pure film shows an increase in the charge transfer resistance under illumination, which means that the photogenerated holes could accumulate on the surface of the photoanode but they were not transferred to the water. An extrapolation of the complex diagram of the films presents that

Table 1 Parameters of Mott-Schottky and band gap analyses of $BiVO_4$ and $BiVO_4$/FeOOH films

Parameters	$BiVO_4$	$BiVO_4$/FeOOH
E_{fb} (V vs. RHE)	0.86	0.82
N_D (cm^{-3})	1.09×10^{20}	5.38×10^{19}
Semiconductor type	n	n
E_g (eV)	2.59	2.57
Conduction band potential, E_{CB} (V vs. RHE)	0.86	0.82
Valence band potential, E_{VB} (V vs. RHE)	3.45	3.39

the charge transfer resistance of the $BiVO_4$ is approximately 8.5 times higher than the $BiVO_4$/FeOOH. Hence, the FeOOH decreases of the charge transfer resistance from the $BiVO_4$ to the electrolyte because the holes are probably transferred to iron first and then from the FeOOH to the H_2O. This hypothesis is in agreement with the mediation in the charge transfer that the centers containing the Fe (II)-Fe (III) performed, as proposed with the green rust formation during the photoelectrodeposition of the FeOOH on the $BiVO_4$ surface, and as represented in Fig. 8b. Ding et al. [47] observed a similar behavior when studying the effect of cobalt borate deposition on the $BiVO_4$. The authors showed a decrease in the charge transfer resistance with a cobalt borate top layer.

In fact, the same behavior has been exhibited by other oxyhydroxides with different metals as Ni [24, 48], Co [49], Mn [50, 51] and their borates [7, 47], phosphates [52], or a mixture of these [24, 53] when they are deposited on a light absorber layer. However, we think that if the FeOOH acts strictly as a catalyst, then the onset photocurrent could be significantly shifted to negative potentials and the voltammetric profile could exhibit photocurrent saturation. Remember that we did not observe a shift of the onset potential to the $BiVO_4$/FeOOH photocurrent when compared to pure $BiVO_4$. Therefore, it is more appropriate for the FeOOH to operate as a charge transfer mediator. Probably, the FeOOH might have a large density of non-stoichiometric defects, and this contributes to increasing the charge transfer kinetics. The same explanation has been suggested for other metallic oxyhydroxides and phosphates [24, 52, 54]. However, it is important to note that all of these compounds have metallic centers that can present different oxidation states.

Besides the role of the FeOOH as the center of charge transfer mediation, this material could passive the surface states of the $BiVO_4$ as the E_{ocp} shifted 70 mV to more positive potentials. Kim et al. [29] also reported the phenomenon of the passivation of the surface state of the Fe_2O_3 by the FeOOH. Another possibility of green rust mechanism in the photoelectrochemical water oxidation is the enhancement of the charge separation, which occurs because the iron oxyhydroxide layer could work as a blocking layer. Such behavior was studied by Gromboni et al. [55] applying Al_2O_3 as a blocking layer on $BiVO_4$. The authors demonstrated a potential applied dependence with the mechanism of photocurrent generation after Al_2O_3 thin layer deposition. In a low bias potential, the photocurrent increases because the

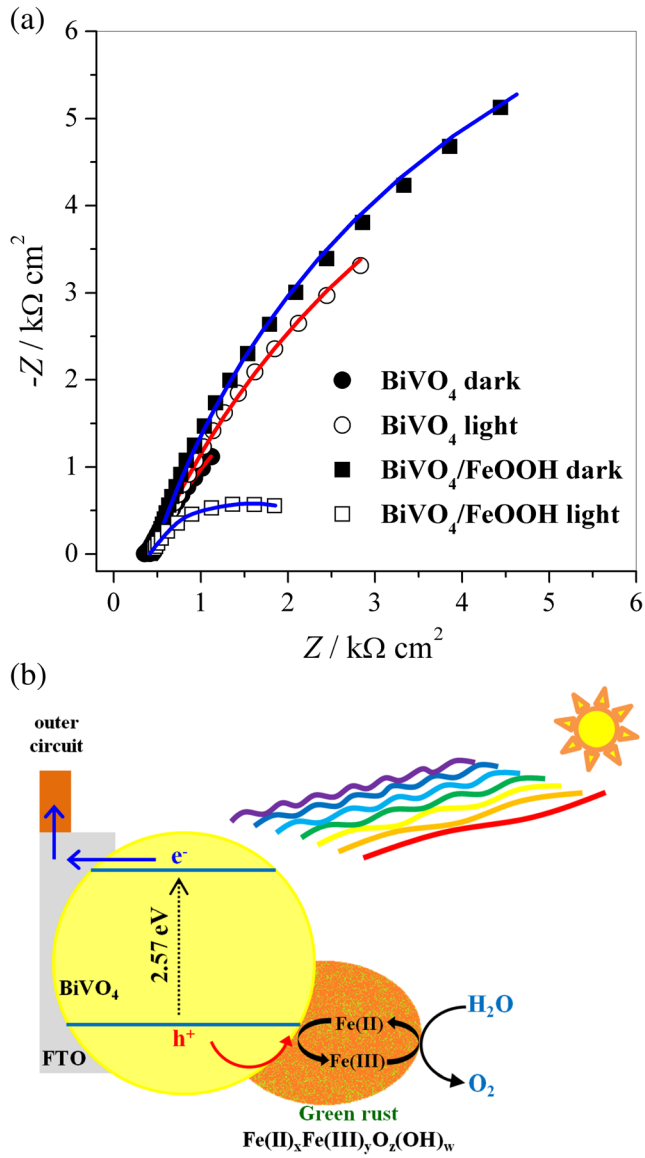

Fig. 8 **a** Complex plane diagram under dark and sun light simulator at open circuit potential of $BiVO_4$ and $BiVO_4$/FeOOH films. Measurements performed in Na_2SO_4 0.5 mol L^{-1} pH 5.6. The solid lines represent the extrapolation. **b** Schematic band diagram of the $BiVO_4$/FeOOH photoanode under illumination, CB, conduction band, VB, valence band, e^-, electron, and h^+, hole photogenerated

charge recombination of electrons with oxygen (produced by water oxidation and diffused through the film) and of electron with holes is suppressed. In a high bias potential, the charge carrier mobility is increased due to the Al_2O_3, which declines the surface states compared to the bare $BiVO_4$. Finally, we present here a simple method of $BiVO_4$ deposition that after the photoelectrodeposition of the FeOOH on the photoanode increases the value of the photocurrent density 3.4 times.

Conclusions

$BiVO_4$ films were produced with a thickness of around 700 nm in a simple way employing a spin-coating deposition and a mixture of solutions of $Bi(NO_3)_3$ 0.4 mol L^{-1} and NH_4VO_3 0.4 mol L^{-1} dissolved into polyethylene glycol 300 and ethylene glycol 1:1 (v:v). After the photoelectrodeposition of the FeOOH was observed an increase in the photocurrent density of 3.4 times, whereas shifting in the onset photocurrent density was not noted, this implies that the FeOOH works as a charge transfer mediator. In addition, this material can passive the surface state of the $BiVO_4$ as the E_{ocp} shifts toward positive potentials. The $BiVO_4$ presents the pure monoclinic phase, which was evidenced by X-ray diffraction and the optical band gap estimated was 2.59 eV. With the overlay of the FeOOH no significant changes in the diffraction patterns, or band gap of photoanode were observed. Furthermore, the FeOOH does not present diffraction peaks evidencing a crystalline phase; however it is possible to recognize the small particles on the $BiVO_4$ through SEM images. The electrochemical impedance spectroscopy showed that the FeOOH decreases the charge transfer resistance. The Mott-Shottky plots revealed that the E_{fb} shifted toward more potential when modifying the $BiVO_4$ surface with the FeOOH, and the carrier densities did not change significantly. The photoelectrochemical data presented here led us to believe that the FeOOH acts strictly as a charge transfer mediator and not as an oxygen evolution catalyst.

Acknowledgements This work was supported by São Paulo Research Foundation (CEPID/FAPESP process 2013/07296-2, grant 2016/12681-0), the National Council of Technological and Scientific Development (CNPq, grants for M.A. de Araújo and D. Coelho), and the Coordination for the Improvement of Higher Education Personnel (CAPES, grant PNPD for D. Coelho).

References

1. Fushima A, Honda K (1972) Electrochemical photolysis of water at a semiconductor electrode. Nature 238:37–38
2. da Silva MR, Lucilha AC, Afonso R, Dall'Antonia LH, Scalvi LVD (2014) Photoelectrochemical properties of FTO/m-BiVO4 electrode in different electrolytes solutions under visible light irradiation. Ionics 20(1):105–113
3. Xu J, Wang WZ, Wang J, Liang YJ (2015) Controlled fabrication and enhanced photocatalystic performance of BiVO4@CeO2 hollow microspheres for the visible-light-driven degradation of rhodamine B. Appl Surf Sci 349:529–537
4. Obregon S, Colon G (2015) On the origin of the photocatalytic activity improvement of BIVO4 through rare earth tridoping. Appl Catal a-Gen 501:56–62
5. Chen L, Alarcon-Llado E, Hettick M, Sharp ID, Lin YJ, Javey A, Ager JW (2013) Reactive sputtering of bismuth vanadate photoanodes for solar water splitting. J Phys Chem C 117(42): 21635–21642
6. Cho SK, Park HS, Lee HC, Nam KM, Bard AJ (2013) Metal Doping of BiVO4 by composite electrodeposition with improved photoelectrochemical water oxidation. J Phys Chem C 117(44): 23048–23056
7. Choi SK, Choi W, Park H (2013) Solar water oxidation using nickel-borate coupled BiVO4 photoelectrodes. Phys Chem Chem Phys 15(17):6499–6507
8. Luo WJ, Li ZS, Yu T, Zou ZG (2012) Effects of surface electrochemical pretreatment on the photoelectrochemical performance of Mo-doped BiVO4. J Phys Chem C 116(8):5076–5081
9. Pilli SK, Furtak TE, Brown LD, Deutsch TG, Turner JA, Herring AM (2011) Cobalt-phosphate (Co-Pi) catalyst modified Mo-doped BiVO4 photoelectrodes for solar water oxidation. Energy Environ Sci 4(12):5028–5034
10. Guo F, Shi WL, Lin X, Che GB (2014) Hydrothermal synthesis of graphitic carbon nitride-BiVO4 composites with enhanced visible light photocatalytic activities and the mechanism study. J Phys Chem Solids 75(11):1217–1222
11. Lei BX, Zhang P, Wang SN, Li Y, Huang GL, Sun ZF (2015) Additive-free hydrothermal synthesis of novel bismuth vanadium oxide dendritic structures as highly efficient visible-light photocatalysts. Mat Sci Semicon Proc 30:429–434
12. Liu X, Liu Y, Su JZ, Li MT, Guo LJ (2015) Facile preparation of BiVO4 nanoparticle film by electrostatic spray pyrolysis for photoelectrochemical water splitting. Int J Hydrogen Energ 40(38):12964–12972
13. Liang ZT, Cao YL, Qin HY, Jia DZ (2016) Low-heating solid-state chemical synthesis of monoclinic scheelite BiVO4 with different morphologies and their enhanced photocatalytic property under visible light. Mater Res Bull 84:397–402
14. Ravidhas C, Josephine AJ, Sudhagar P, Devadoss A, Terashima C, Nakata K, Fujishima A, Raj AME, Sanjeeviraja C (2015) Facile synthesis of nanostructured monoclinic bismuth vanadate by a co-precipitation method: structural, optical and photocatalytic properties. Mat Sci Semicon Proc 30:343–351
15. Alarcon-Llado E, Chen L, Hettick M, Mashouf N, Lin YJ, Javey A, Ager JW (2014) BiVO4 thin film photoanodes grown by chemical vapor deposition. Phys Chem Chem Phys 16(4):1651–1657
16. Mascaro LH, Pockett A, Mitchels JM, Peter LM, Cameron PJ, Celorrio V, Fermin DJ, Sagu JS, Wijayantha KGU, Kociok-Kohn G, Marken F (2015) One-step preparation of the BiVO4 film photoelectrode. J Solid State Electr 19(1):31–35
17. Eda S, Fujishima M, Tada H (2012) Low temperature-synthesis of BiVO4 nanorods using polyethylene glycol as a soft template and the visible-light-activity for copper acetylacetonate decomposition. Appl Catal B-Environ 125:288–293
18. He HC, Berglund SP, Rettie AJE, Chemelewski WD, Xiao P, Zhang YH, Mullins CB (2014) Synthesis of BiVO4 nanoflake array films for photoelectrochemical water oxidation. J Mater Chem A 2(24): 9371–9379
19. Zhou B, Qu JH, Zhao X, Liu HJ (2011) Fabrication and photoelectrocatalytic properties of nanocrystalline monoclinic BiVO4 thin-film electrode. J Environ Sci-China 23(1):151–159
20. Wang DE, Li RG, Zhu J, Shi JY, Han JF, Zong X, Li C (2012) Photocatalytic water oxidation on BiVO4 with the electrocatalyst as

an oxidation cocatalyst: essential relations between electrocatalyst and photocatalyst. J Phys Chem C 116(8):5082–5089
21. Abdi FF, van de Krol R (2012) Nature and light dependence of bulk recombination in Co-Pi-catalyzed BiVO4 photoanodes. J Phys Chem C 116(17):9398–9404
22. Luo WJ, Yang ZS, Li ZS, Zhang JY, Liu JG, Zhao ZY, Wang ZQ, Yan SC, Yu T, Zou ZG (2011) Solar hydrogen generation from seawater with a modified BiVO4 photoanode. Energy Environ Sci 4(10):4046–4051
23. Kim JH, Jang JW, Kang HJ, Magesh G, Kim JY, Kim JH, Lee J, Lee JS (2014) Palladium oxide as a novel oxygen evolution catalyst on BiVO4 photoanode for photoelectrochemical water splitting. J Catal 317:126–134
24. Kim TW, Choi KS (2014) Nanoporous BiVO4 photoanodes with dual-layer oxygen evolution catalysts for solar water splitting. Science 343(6174):990–994
25. Seabold JA, Choi KS (2012) Efficient and stable photo-oxidation of water by a bismuth vanadate photoanode coupled with an iron oxyhydroxide oxygen evolution catalyst. J Am Chem Soc 134(4): 2186–2192
26. Park Y, Kang D, Choi KS (2014) Marked enhancement in electron-hole separation achieved in the low bias region using electrochemically prepared Mo-doped BiVO4 photoanodes. Phys Chem Chem Phys 16(3):1238–1246
27. McDonald KJ, Choi KS (2012) A new electrochemical synthesis route for a BiOI electrode and its conversion to a highly efficient porous BiVO4 photoanode for solar water oxidation. Energy Environ Sci 5(9):8553–8557
28. Chen L, Toma FM, Cooper JK, Lyon A, Lin YJ, Sharp ID, Ager JW (2015) Mo-Doped BiVO4 photoanodes synthesized by reactive sputtering. ChemSusChem 8(6):1066–1071
29. Kim JY, Youn DH, Kang K, Lee JS (2016) Highly conformal deposition of an ultrathin FeOOH layer on a hematite nanostructure for efficient solar water splitting. Angew Chem Int Edit 55(36): 10854–10858
30. Ishihara H, Kannarpady GK, Khedir KR, Woo J, Trigwell S, Biris AS (2011) A novel tungsten trioxide (WO_3)/ITO porous nanocomposite for enhanced photo-catalytic water splitting. Phys Chem Chem Phys 13:19553–19560
31. Ren K, Gan YX, Nikolaidis E, Sofyani SA, Zhang L (2013) Electrolyte concentration effect of a photoelectrochemical cell consisting of TiO_2 nanotubes anode. ISRN Materials Science 2013: 682516
32. Hill JC, Choi KS (2012) Effect of electrolytes on the selectivity and stability of n-type WO_3 photoelectrodes for use in solar water oxidation. J Phys Chem C 116:7612–7620
33. Monfort O, Pop L-C, Sfaelou S, Plecenik T, Roch T, Dracopoulos V, Stathatos E, Plesch G, Lianos P (2016) Photoelectrocatalytic hydrogen production by water splitting using $BiVO_4$ photoanodes. Chem Eng J 286:91–97
34. Luo WJ, Wang ZQ, Wan LJ, Li ZS, Yu T, Zou ZG (2010) Synthesis, growth mechanism and photoelectrochemical properties of BiVO4 microcrystal electrodes. J Phys D Appl Phys 43(40):405402
35. Bolzan AA, Fong C, Kennedy BJ, Howard CJ (1997) Structural studies of rutile-type metal dioxides. Acta Crystallogr B 53:373–380
36. Noyan IC, Huang TC, York BR (1995) Residual stress/strain snalysis in thin films by X-ray diffraction. Crit Rev Solid State 20(2):125–177
37. Kim TW, Choi KS (2016) Improving stability and photoelectrochemical performance of BiVO4 photoanodes in basic media by adding a ZnFe2O4 layer. J Phys Chem Lett 7(3):447–451
38. Nowak M, Kauch B, Szperlich P (2009) Determination of energy band gap of nanocrystalline SbSI using diffuse reflectance spectroscopy. Rev Sci Instrum 80(4):046107
39. Seabold JA, Zhu K, Neale NR (2014) Efficient solar photoelectrolysis by nanoporous Mo: BiVO4 through controlled electron transport. Phys Chem Chem Phys 16(3):1121–1131
40. Chemelewski WD, Lee HC, Lin JF, Bard AJ, Mullins CB (2014) Amorphous FeOOH oxygen evolution reaction catalyst for photoelectrochemical water splitting. J Am Chem Soc 136(7): 2843–2850
41. Genin JMR, Olowe AA, Refait P, Simon L (1996) On the stoichiometry and Pourbaix diagram of Fe (II)-Fe (III) hydroxy-sulphate or sulphate-containing green rust 2: an electrochemical and Mossbauer spectroscopy study. Corros Sci 38(10):1751–1762
42. Refait P, Drissi SH, Pytkiewicz J, Genin JMR (1997) The anionic species competition in iron aqueous corrosion: role of various green rust compounds. Corros Sci 39(9):1699–1710
43. Sarkar S, Chattopadhyay KK (2012) Size-dependent optical and dielectric properties of BiVO4 nanocrystals. Phys E 44(7–8): 1742–1746
44. Finklea HO (1988) Studies in physical and theoretical chemistry. In: Semiconductor electrodes, vol 55. Elsevier, Amsterdam
45. Liu CJ, Li J, Li YM, Li WZ, Yang YH, Chen QY (2015) Epitaxial growth of Bi2S3 nanowires on BiVO4 nanostructures for enhancing photoelectrochemical performance. RSC Adv 5(88):71692–71698
46. Hong SJ, Lee S, Jang JS, Lee JS (2011) Heterojunction BiVO4/WO3 electrodes for enhanced photoactivity of water oxidation. Energy Environ Sci 4(5):1781–1787
47. Ding CM, Shi JY, Wang DG, Wang ZJ, Wang N, Liu GJ, Xiong FQ, Li C (2013) Visible light driven overall water splitting using cocatalyst/BiVO4 photoanode with minimized bias. Phys Chem Chem Phys 15(13):4589–4595
48. Lin FD, Boettcher SW (2014) Adaptive semiconductor/electrocatalyst junctions in water-splitting photoanodes. Nat Mater 13(1):81–86
49. Jia QX, Iwashina K, Kudo A (2012) Facile fabrication of an efficient BiVO4 thin film electrode for water splitting under visible light irradiation. P Natl Acad Sci USA 109(29):11564–11569
50. Zaharieva I, Chernev P, Risch M, Klingan K, Kohlhoff M, Fischer A, Dau H (2012) Electrosynthesis, functional, and structural characterization of a water-oxidizing manganese oxide. Energy Environ Sci 5(5):7081–7089
51. Nam KM, Cheon EA, Shin WJ, Bard AJ (2015) Improved photoelectrochemical water oxidation by the WO3/CuWO4 composite with a manganese phosphate electrocatalyst. Langmuir 31(39):10897–10903
52. Abdi FF, Firet N, van de Krol R (2013) Efficient BiVO4 thin film photoanodes modified with Cobalt Phosphate catalyst and W-doping. ChemCatChem 5(2):490–496
53. Roger I, Symes MD (2016) First row transition metal catalysts for solar-driven water oxidation produced by electrodeposition. J Mater Chem A 4(18):6724–6741
54. Kanan MW, Nocera DG (2008) In situ formation of an oxygen-evolving catalyst in neutral water containing phosphate and Co2+. Science 321(5892):1072–1075
55. Gromboni MF, Coelho D, Mascaro LH, Pockett A, Marken F (2017) Enhancing activity in a nanostructured BiVO4 photoanode with a coating of microporous Al2O3. Appl Catal B Environ 200: 133–140